ORIGINAL PAPER

Convergence of the electronic density for a target region in cluster models of a NH₃ molecular crystal

Anders Hutcheson[1] · Ida-Marie Høyvik[1]

Abstract

In this paper we illustrate the advantage of addressing size-intensive properties of target regions without first converging the ground-state energy of that region. We use local occupied and virtual orbitals to separate the orbital space of NH_3 clusters into an orbital space for the target region (a central NH_3 molecule) and for the remaining cluster. Convergence characteristics of the Hartree–Fock (HF) energy and, indirectly, the electronic density of the target region are shown. The calculations illustrate that although the energy of the target region will not converge with cluster size, the electronic density will. The convergence of the electronic density of the target region is subsequently exploited to obtain HF dipole moments and CC2-in-HF vertical excitation energies. For these properties convergence is seen upon the inclusion of approximately three shells beyond the target region. This shows that local size-intensive properties of a target region can be investigated without converging the energy. We further show that a minimal basis description of the outer shells are sufficient to capture the correct interaction with the target region. The possibility of computing size-intensive properties for a target region using a converged electronic density, without requiring convergence in the energy itself, is currently an underexploited feature.

Keywords Electronic density · Hartree–Fock · Coupled cluster · Cluster model · Molecular crystal · Local properties · Local orbitals

✉ Ida-Marie Høyvik
  ida-marie.hoyvik@ntnu.no

  Anders Hutcheson
  anders.hutcheson@ntnu.com

[1] Department of Chemistry, The Norwegian University of Science and Technology, Høgskoleringen 5, 7491 Trondheim, Norway

1 Introduction

In 1996 Kohn [1] introduced the term "nearsightedness" of electrons in many-atom systems. This feature describes that local electronic properties, such as the electronic density, depend significantly on the effective external potential only at nearby points. The convergence of the electronic density for a local region has also been discussed by others [2–5]. The feature has been exploited to develop numerous linear-scaling electronic structure models and embedding schemes. However, unlike the electronic density, the ground-state electronic energy is not nearsighted. Hence, for systems such as molecular crystals, the energy of a target region requires the infinite surroundings to be taken into account, thus motivating the use of periodic boundary conditions. A target region may be a unit cell, single molecule or group of molecules in the crystal. Since the constituents of molecular crystals are molecules, wave function models originally developed for single molecules have therefore been extended to periodic codes. Notable examples are the plane wave periodic MP2 method [6] implemented in VASP, the periodic divide-expand-consolidate MP2 method developed by Pedersen et al. [7], the periodic MP2 and CCSD developed by McClain et al. [8], and the local MP2 method [9] available in the Cryscor program.

To achieve linear-scaling wavefunctions for molecular systems, local molecular orbital (MO) spaces are often used. Explicit localization of occupied MOs has been a popular topic for many decades, with seminal contributions such as the widely used Edmiston-Ruedenberg [10], Foster-Boys [11], and Pipek-Mezey [12] localization functions. In addition to explicit localization, several approaches for generating local virtual spaces exist such as projected atomic orbitals (PAOs) [13], pair-natural orbitals [14–16] and correlated natural transition orbitals [17]. However, for the infinite molecular crystals orbital space locality faces two challenges (i) orthogonalization tails and (ii) near-linear dependencies.

Orthogonalization tails compromise compactness of the description, since for a given region in space, local MOs outside the region will be required to have components inside the region due to the orthogonality requirement. Using high-quality atomic orbital (AO) basis sets, there is a large number of MOs centered far outside the given region which must have components inside the region. Parts of the orbital space in a given region is therefore spanned by MOs centered outside the region. These components may cause the correlation energy to converge slowly in local correlation approaches relative to when non-orthogonal orbitals such as the PAOs are used. This is seen in the results presented by Werner and collaborators [18] and is explicitly shown by Hansen et al. [19]. The results of Hansen et al. indicate that some issues concerning orthogonalization tails may be circumvented by using PAOs rather than local virtual MOs (or Wannier orbitals).

With respect to near-linear dependencies, AOs are per construction designed to describe atoms in free space, and for large or dense systems the concerted effect of AOs on different atomic centers greatly enhances near-linear dependencies.

Near-linear dependencies will not appreciably affect the locality of the occupied space, but the virtual space will be severely affected [20]. Dealing with near-linear dependencies in a periodic framework may compromise the basis set quality, since removing AOs from the unit cell will remove AOs from all unit cells. While near-linear

dependencies can be avoided by using plane wave basis sets, there are other problems with this approach, such as the need for a high energy cut-off to achieve accurate results.

When targeting local size-intensive properties of molecular crystals, the nearsightedness of electrons may allow the use of cluster models. Cluster models enables different basis sets to be used in different regions of the cluster. Hence one may use smaller basis sets outside a target region. The problems of orthogonalization tails and near-linear dependencies may therefore be alleviated by using cluster models. Further, cluster models allows for any molecular wave function based scheme to be used for its description. Due to the nearsightedness of the electronic density, local size-intensive properties in a target region may be converged with cluster size. The traditional approach would be to first compute the converged energy, however, the energy of the target region will not be converged for reasonably sized clusters. Therefore, if one does not aim to converge the energy with cluster size, any existing fragment or orbital based correlated wave function models [21–42] can be used to compute size-intensive properties of the target region.

In this paper, we illustrate that one may obtain converged size-intensive properties of a target region without converging the energy of the target region. Cluster models of various sizes gives us the opportunity to show how electronic properties converge with increasing cluster size. Furthermore, the cluster models allows us to explore how choice of basis set outside the target region affects the computed properties. One possibility being to choose a high-quality basis set in and around the region of interest, while low-quality basis sets (such as minimal basis) may be used further out in the cluster model. A minimal basis does not exhibit flexibility to describe accurate molecular properties, but it may adequately describe long-range effects between the electronic density of the targeted region and the electronic density far away. The aim of this paper is therefore not to obtain accurately computed electronic properties, but rather to illustrate fundamental concepts related to the convergent nature of the electronic density and how it may be exploited.

The paper is organized as follows. In Sect. 2 we provide a theoretical background on how to partition the energy in terms of a target region and the remainder of the cluster, as well as an argument from an optimization vantage point for why the electronic density should converge with cluster size. In Sect. 3 we present computational details and describe the cluster models of an NH_3 molecular crystal, and in Sect. 4 we present numerical illustrations using these cluster models. A summary and concluding remarks is given in Sect. 5.

2 Theoretical background

In this section we present equations and background for the partitioning of the Hartree–Fock electronic energy in terms of a partitioning of a fully optimized Hartree–Fock density matrix for the cluster. The density and energy partitioning used was introduced by Høyvik et al. [43] for multilevel Hartree–Fock. We note that the partitioning is used to illustrate the convergence behaviour of the energy. The partitioning used here is not a requirement for computing size-intensive properties of a target-region, as one may

use any existing fragmentation or orbital space partitioning approach for this. The only requirement is that the approach allows for the effective interaction of the target region with the rest of the cluster. After presenting the partioning of the energy, we discuss why it is reasonable to assume that the electronic density of a target region will converge with cluster size by analyzing the optimization procedure from a local perspective rather than a canonical (diagonalization based) perspective.

2.1 Energy partitioning

We consider a cluster model of a molecular crystal where the total electronic density for the cluster is given by $\mathbf{D} = \mathbf{D}_t + \mathbf{D}_r$. $\mathbf{D}_t$ is the density of the target region, and $\mathbf{D}_r$ is the remainder of the density. The total density $\mathbf{D}$ is the Hartree–Fock density matrix for the full cluster. All three densities, $\mathbf{D}$, $\mathbf{D}_t$ and $\mathbf{D}_r$ satisfy the trace, symmetry and idempotence criteria of density matrices representing Slater determinants, i.e. $\mathbf{D}_t$ and $\mathbf{D}_r$ can be viewed as constructed from separate subsets of orthogonal MOs describing the full density matrix $\mathbf{D}$. The electronic energy (excluding nuclear repulsion) for the target region described by $\mathbf{D}_t$, interacting with the rest of the cluster described by $\mathbf{D}_r$ is given by,

$$
\begin{aligned}
E_t &= \mathrm{Tr}[\mathbf{h}\mathbf{D}_t] + \frac{1}{4}\mathrm{Tr}[\mathbf{D}_t\mathbf{G}(\mathbf{D}_t)] + \frac{1}{2}\mathrm{Tr}[\mathbf{D}_t\mathbf{G}(\mathbf{D}_r)] \\
&\equiv E_t^{1\text{-el}} + E_t^{2\text{-el}} + E_t^{\text{int}},
\end{aligned}
\tag{1}
$$

where we have defined $E_t^{1\text{-el}}$, $E_t^{2\text{-el}}$ and E_t^{int} as the one-electron, two-electron and interaction contributions, respectively. Two-electron and interaction terms are defined through the $\mathbf{G}$ matrix which in the MO basis is defined through elements

$$
G(\mathbf{M})_{ij} = \sum_{kl}(2g_{ijkl} - g_{ilkj})M_{kl},
\tag{2}
$$

where we have introduced two-electron integrals in the Mulliken notation

$$
g_{ijkl} = \int\int \phi_i^*(\mathbf{r}_1)\phi_j(\mathbf{r}_1)\frac{1}{r_{12}}\phi_k^*(\mathbf{r}_2)\phi_l(\mathbf{r}_2)d\mathbf{r}_1 d\mathbf{r}_2.
\tag{3}
$$

The electronic part of the Hartree–Fock energy (nuclear repulsion excluded) of the full cluster is given by

$$
E = E_t + \mathrm{Tr}[\mathbf{h}\mathbf{D}_r] + \frac{1}{4}\mathrm{Tr}[\mathbf{D}_r\mathbf{G}(\mathbf{D}_r)],
\tag{4}
$$

i.e., the energy for the target region, E_t, plus the contributions which only depend on $\mathbf{D}_r$. Note that all two-electron interactions between the target region and the rest of the cluster is included in E_t.

As is well-known, the energy of a target region in an infinite (or similarly, large) system, is not a local quantity even if the target density matrix $\mathbf{D}_t$ is localized in space.

The reason for this is long-range interactions between the local target density and nuclei and between the local target density and the electron density of the rest of the system. Hence, the energy of the target region E_t will not converge appreciably for finite cluster sizes. This is well recognized and part of the motivation behind periodic treatments of infinite systems. However, an important point here is that the lack of convergence of the energy with system size does not necessarily reflect a lack of convergence for the electronic density in the target region. In the next section we present an optimization viewpoint of why the electronic density of a target region in a finite cluster of a molecular crystal converges with cluster size.

2.2 Density convergence

For the optimization of a Hartree–Fock state, diagonalization (Roothaan–Hall) based schemes are widely used. However, the diagonalization based schemes impose extra restrictions on the MOs to generate a diagonal Fock matrix (through canonical orbitals) whereas the optimization condition only requires a block-diagonal Fock matrix. To investigate the effect on the target electronic density by the increasing cluster size, it is instructive to consider an optimization based scheme which does not enforce a canonical basis. Hence, we look at a scheme based on an exponential parametrization of MO coefficients [44, 45], where in each iteration new orbitals are generated by a unitary transformation,

$$\tilde{\mathbf{C}} = \mathbf{C}\exp(\boldsymbol{\kappa}). \tag{5}$$

The anti-symmetric parameter matrix $\boldsymbol{\kappa}$ contains only non-redundant parameters, i.e., only the occupied-virtual blocks of $\boldsymbol{\kappa}$ are non-zero for a closed-shell state. A quadratic model of the total energy for the cluster can then be constructed, giving a linear-equation Newton based optimization scheme where in each Hartree–Fock iteration, we solve the linear equation

$$\mathbf{H}\boldsymbol{\kappa} = -\mathbf{G}. \tag{6}$$

Therefore, the solution in each iteration formally is given by,

$$\boldsymbol{\kappa} = -\mathbf{H}^{-1}\mathbf{G}, \tag{7}$$

although the equations are usually solved in an reduced space (iterative) manner. $\mathbf{H}$ and $\mathbf{G}$ are the electronic Hessian and gradient, respectively. In the (non-canonical) orbital basis the electronic Hessian is [46]

$$H_{ai,bj} = 4(\delta_{ij}F_{ab} - \delta_{ab}F_{ij} + 4g_{aibj} - g_{abij} - g_{ajib}), \tag{8}$$

where F_{pq} are elements of the MO Fock matrix, and the electronic gradient is [46]

$$G_{ai} = -4F_{ai}. \tag{9}$$

Exploiting that the electronic Hessian is diagonally dominant, we may write the orbital rotation parameters approximately as

$$\kappa_{ai} \approx -H_{ai,ai}^{-1} G_{ai} = 4H_{ai,ai}^{-1} F_{ai}. \tag{10}$$

The diagonal Hessian elements are $H_{ai,ai} = 4(F_{aa} - F_{ii} + 4g_{aiai} - g_{aaii} - g_{aiia})$ and their magnitude is therefore dominated by the difference $F_{aa} - F_{ii}$. Hence, $H_{ai,ai}^{-1}$ will not be a divergent term for systems with non-vanishing HOMO–LUMO gaps, since $F_{aa} - F_{ii}$ will for such systems always be of a reasonable size. Close to convergence of the Hartree–Fock state, the occupied-virtual Fock matrix element F_{ai} will be small since these are gradient terms, but far from convergence (in the initial Hartree–Fock iterations), F_{ai} will generally have a significant size.

For illustrative purposes, we now assume that in each Hartree–Fock iteration we have an orbital basis of local occupied and virtual MOs. For molecular systems (including cluster models of molecular crystals) with non-vanishing HOMO–LUMO gaps we know that such a basis exists, and in principle we can for each iteration use redundant orbital rotations to generate such a basis. In each iteration the resulting new occupied orbital i can be written as

$$\tilde{C}_{\mu i} = C_{\mu i} + \sum_a C_{\mu a} \kappa_{ai} + \mathcal{O}(\kappa^2) \tag{11}$$

Hence, for each iteration in the energy optimization, an orbital i in the target region will get an amount of virtual MO a mixed in, weighted (to first order) by the magnitude of κ_{ai}. Hence, if an occupied MO i (and hence, the electronic density) is to be changed by a virtual orbital a centered far away, κ_{ai} must be of a significant size. If we look at Eq. (10), we see that the size of κ_{ai} will be determined by the size of F_{ai}. For local orbitals i and a centered far away from each other F_{ai} exhibits a rapid decay [47] and therefore the MOs of the target region (and thus the density of the target region) will at some point be unchanged when increasing the cluster size. The use of local MOs in this analysis is convenient from a conceptual point of view since local MOs also enable a partitioning into a target density which is local. However, the density is invariant with respect to redundant rotations, and the convergence properties of a local part of the density with cluster size is indifferent to choice of basis.

3 Methodology

In this section we present computational details, description of the NH$_3$ molecular clusters used and how the active excitation space for CC2-in-HF calculations are chosen.

3.1 Computational details

LSDalton [48] was used for the Hartree–Fock calculations and subsequent localization of the occupied orbitals. For the Hartree–Fock calculation, the screening threshold for

the integral evaluation was set to 10^{-10} and convergence threshold was set to 10^{-8}. The localization of the occupied orbitals is done by using the second power of the second central moment localization function [49]. CC2-in-HF excitation energies were computed in eT [50], by using the local orbitals obtained from LSDalton. For CC2-in-HF the CC2 wave function is constructed in a subset of the full orbital space whereas interaction with the inactive space (frozen Hartree–Fock orbitals) enters through the Fock matrix. For details see Ref. [50]. The frozen core approximation was used for all CC2-in-HF calculations. The decomposition of the electron repulsion integrals [51] threshold was set to 10^{-5}. The energy and residual thresholds for the coupled cluster ground state were set to 10^{-7}, and the residual threshold for the coupled cluster excited states were set to 10^{-3}.

3.2 Description of NH_3 molecular clusters

In this paper we look at cluster models of crystalline NH_3 (crystal structure obtained from Ref. [52]). Clusters comprised of 13, 40, 143, 324, 579 and 953 molecules are used and the models represent a target region (central NH_3 molecule) with a certain number of shells. The clusters are depicted in Fig. 1, as well as how the cluster is
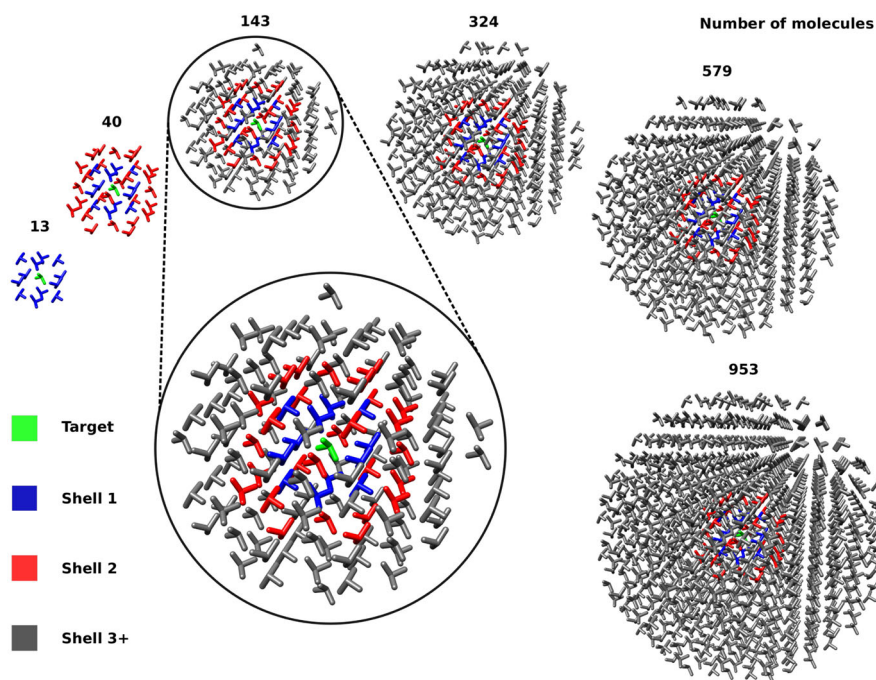

Fig. 1 The ammonia clusters used, with the regions where different basis set can be used colored. The target region (green) is the central NH_3 molecule, shell 1 (blue) is the first shell of 12 molecules, shell 2 (red) is the second shell of 27 molecules, while shell 3+ (grey) is any shells beyond the second shell. In the target region aug-cc-pVTZ is always used, the basis sets of shell 1 and shell 2 are variable, and STO-3G is always used for shell 3+ (Color figure online)

divided into regions where different basis sets may be used. In the target region we always use the aug-cc-pVTZ basis set [53], while for shell 1 and shell 2 we vary the choice of basis set. For shells beyond shell 2, hereby termed shell 3+, STO-3G [54] is always used. When augmented basis sets are used, augmentation is only included for nitrogen atoms, and the non-augmented version of the basis set is used on hydrogen atoms.

3.3 Orbital space partitioning

We use local occupied MOs generated by a trust-region minimization [55] of the second power of the second central moment [49] localization function. The occupied orbital space is partitioned based on the centers, defined by the expectation value of the orbital position vector ($\langle \phi_i \mid \hat{x} \mid \phi_i \rangle$, $\langle \phi_i \mid \hat{y} \mid \phi_i \rangle$, $\langle \phi_i \mid \hat{z} \mid \phi_i \rangle$), of the local MOs. An occupied MO ϕ_i belongs to the region (target, shell 1, etc.) to which it is situated closest to, as defined by the l_2 norm of the difference between the orbital position vector and the atomic positions. For the virtual space, we use the projected atomic orbitals (PAOs) generated for the virtual active region of the cluster (see Sect. 3.4).

3.4 The excitation space for CC2-in-HF calculations

The vertical $S_0 \rightarrow S_1$ excitation energies presented here are computed using a fixed occupied CC2 active space, where only occupied orbitals centered in the target region is included. To be able to investigate the convergence of the excitation energies with an increasing virtual space, in addition to cluster size, we define two different CC2 active virtual regions; target + shell 1 and target + shell 1-2. The inclusion of a larger occupied space would allow for relaxation effects in the occupied space yielding lower excitation energies. However, the purpose of this study is to explore the effect of cluster size and basis set for the excitation energies. We note that the target region approach is only useful for size-intensive (local) properties.

4 Numerical illustrations using NH₃ clusters

In this section we use the NH_3 clusters described in Sect. 3.2 to illustrate effects of cluster size on the energy and the electronic density in the target region (the central NH_3 molecule). The convergence of the electronic density will indirectly be illustrated through presenting results for the Hartree–Fock electric dipole moment and CC2 $S_0 \rightarrow S_1$ vertical excitation energies for the target region. Further, we will explore how these properties depends on the quality of the basis set outside the target region (shell 1 and shell 2).

4.1 Effect of cluster size

4.1.1 Target region energy versus target region electronic density

In this section we present Hartree–Fock calculations on clusters comprised of 13, 40, 143, 324, 579 and 953 NH_3 molecules where an orbital space partitioning (see Sect. 3.3) of the Hartree–Fock orbital space is used to divide the system into a density for the target region and the remainder density. The basis sets used are aug-cc-pVTZ in the target region (central NH_3 molecule), aug-cc-pVDZ for shell 1, STO-3G for shell 2 and STO-3G for shell 3+, see Sect. 3.2 for a description of the clusters.

We present the differences in energy contributions (see Sect. 2.1) to the target region energy for increasing cluster size. I.e., we present results for

$$\Delta E(m, n) = E^m - E^n \tag{12}$$

where E^m is an energy ($E_t^{1\text{-el}}$, $E_t^{2\text{-el}}$, E_t^{int} or E_t from Eq. (1)) for a cluster containing m molecules and E^n is an energy for a cluster containing n molecules. The results are presented in Table 1. We first consider results for the one-electron contribution, $E_t^{1\text{-el}}$, to the target region. We see that the one-electron energy contribution to the target region energy is increasing in magnitude (but is negative), due to the long-range interaction between the electrons in the target region and all nuclei of the cluster. For the two-electron interaction between the electrons in the target region and the electrons outside the target region, E_t^{int}, we see the same long-range effects, except that here the energy contributions are increasing in magnitude and are of a positive sign. Hence, these energy contributions do not converge with cluster size. However, we see that $\Delta E_t^{1\text{-el}}$ and ΔE_t^{int} have similar values, except with opposite signs. Hence, they nearly cancel each other out. This is seen from the total energy of the target region E_t, where we see that ΔE_t is small, but not converged. On the other hand, we see from Table 1 that $E_t^{2\text{-el}}$ is converging with cluster size. We see that the sign of $\Delta E(m, n)$ for $\Delta E_t^{2\text{-el}}$ switches e.g., between $\Delta E(40, 13)$ and $\Delta E(143, 40)$ and that they are of similar order of magnitude. The same is seen for $\Delta E_t^{2\text{-el}}$ of $\Delta E(324, 142)$ and $\Delta E(579, 324)$. Furthermore, the absolute value $\Delta E(579, 324)$ for $\Delta E_t^{2\text{-el}}$ is seen to be larger than that of $\Delta E(324, 142)$ (0.00037 a.u. versus 0.00019 a.u.). However, considering the increase in number of molecules, the energy differences in terms of change per molecule is of the same size. Looking at $\Delta E_t^{2\text{-el}}$ for the cluster sizes of 953 and 579 molecules, we see that the difference is down to 0.000008 a.u. This implies that, beyond a given cluster size, $\mathbf{D}_t$ is not significantly affected by extending the cluster further. This is a numerical illustration of the theoretical discussion in Sect. 2.2.

4.1.2 Effect of cluster size on dipole moment

In this section we investigate how the cluster size affects the Hartree–Fock electric dipole moment of the target region (central NH_3 molecule). The dipole moment of the target region is computed using the trace of $\mathbf{D}_t$ and the dipole operator. The aug-cc-pVTZ basis set is used in the target region, aug-cc-pVDZ for shell 1, STO-3G for

Table 1 Energy differences Eq. (12) of the energy contributions, $E_t^{1\text{-el}}$, $E_t^{2\text{-el}}$ and E_t^{int} from Eq. (1) as well as their sum, E_t, for ammonia clusters of different sizes

Cluster sizes	$\Delta E_t^{1\text{-el}}$	$\Delta E_t^{2\text{-el}}$	ΔE_t^{int}	ΔE_t
$\Delta E(40, 13)$	− 243.29175	− 0.00252	243.73391	0.43964
$\Delta E(143, 40)$	− 632.16812	0.00242	632.30466	0.13896
$\Delta E(324, 142)$	− 798.07264	− 0.00019	798.07633	0.00349
$\Delta E(579, 324)$	− 896.23328	0.00037	896.20599	− 0.02692
$\Delta E(953, 579)$	− 1102.70560	0.000008	1102.70167	− 0.00392

The clusters are described using aug-cc-pVTZ in the target region (central NH_3 molecule), aug-cc-pVDZ for shell 1, STO-3G for shell 2 and STO-3G for shell 3+, see Sect. 3.2 for a description of the clusters. All values are in a.u

Table 2 Hartree–Fock electric dipole moments (given in Debye) for the target region (central NH_3 molecule), computed for cluster sizes from 13 to 953 ammonia molecules

Cluster size	Dipole moment [D]
13	2.25
40	2.06
143	2.14
324	2.12
579	2.14
953	2.14

The clusters are described using aug-cc-pVTZ in the target region (central NH_3 molecule), aug-cc-pVDZ for shell 1, STO-3G for shell 2 and STO-3G for shell 3+, see Sect. 3.2 for a description of the clusters

shell 2 and STO-3G for shell 3+. The computed dipole moments are given in Table 2. Increasing the cluster size from 13 molecules to 40 molecules reduces the dipole moment by 0.19 D, and increasing the cluster from 40 to 143 molecules increases it by 0.08 D. Increasing the cluster size from 143 to 324 molecules reduces the dipole moment by 0.02 D, and further increases of cluster size gives the same value for the dipole moment as the cluster with 143 molecules. Considering that the mean absolute error in Hartree–Fock dipole moments for molecules is found to be 0.16 D [56], these variations are negligible. Hence, the electric dipole moment of the target region is converged at 143 molecules (target region + 3 shells). This convergence is expected as the results in Table 1 indicate a converged target electronic density matrix.

4.1.3 Effect of cluster size on CC2-in-HF vertical excitation energies

In Table 3 we present CC2-in-HF excitation energies for NH_3 clusters containing 143, 324 and 579 molecules, with the occupied active space restricted to the target region (central NH_3 molecule) and the virtual active restricted to the target region + shell 1 (see Sect. 3.4). The basis set for the target region is aug-cc-pVTZ, whereas the basis set for shell 2 and beyond is STO-3G. For shell 1 we present results using both STO-3G and aug-cc-pVDZ, to see whether the choice of basis in the active virtual region yield different convergence characteristics with cluster size.

Table 3 CC2-in-HF $S_0 \to S_1$ excitation energies (eV) obtained for clusters of 143, 324 and 579 molecules

Basis (shell 1)	143	324	579
STO-3G	9.26	9.24	9.26
aDZ	9.03	9.01	9.03

All calculations are performed with the target region as the active occupied region and the virtual active region set as the target region + shell 1. The basis sets used for the target region is aug-cc-pVTZ and the basis set for shell 2 and beyond is STO-3G

We first consider results where STO-3G was used for shell 1. From Table 3 we see that increasing the cluster size from 143 to 324 molecules the excitation energy is decreased from 9.26 to 9.24 eV. Increasing the cluster size further to 579 molecules changes it back up to 9.26 eV. Using aug-cc-pVDZ for shell 1 we see that the excitation energy is lowered as expected, since more flexibility is added in the active virtual region. However, we see the same convergence behavior as for the calculations where only STO-3G was employed beyond the target region. Hence, for cluster sizes beyond 143 molecules we see that excitation energies oscillates somewhat, but the change is of only 0.02 eV. Considering the intrinsic errors in the CC2 model, the effect on the excitation energy by increasing the cluster size beyond 143 molecule can be considered negligible. In particular, the change in excitation energy of 0.02 eV (= 0.0007 a.u.) should be considered in contrast to the non-converged local region Hartree–Fock energy E_t of the ground state (see Table 1). The absolute differences in E_t for cluster sizes of 143, 324 and 579 molecules are 0.00349 a.u. and 0.02692 a.u. Hence, we see that excitation energies for local excitations may converge with cluster size, even if the ground state energy for the target region does not converge. It is important to note that this does not mean that the presented excitation energies are converged with respect to the chosen active occupied and virtual space. In Sect. 4.2 a study on choice of basis sets is carried out.

4.2 Effect of basis set

4.2.1 Effect of basis set on the Hartree–Fock electric dipole moment

In this section we present how the choice of basis set for shell 1 and 2 affects the dipole moment of the target region (central NH_3 molecule), for a cluster containing 143 molecules. The basis sets of shell 1 and 2 are varied, while for the target region and shell 3+ are kept to aug-cc-pVTZ and STO-3G, respectively. The results are presented in Table 4. If we first consider the results where STO-3G is used for shell 2, Table 4 contain results for using STO-3G, cc-pVDZ, cc-pVTZ, aug-cc-pVDZ and aug-cc-pVTZ. All computed dipole moment values for these basis sets in shell 1 are 2.14–2.15 D. Hence, the target electronic density is not appreciably affected by the choice of basis in shell 1. We next consider the calculations where the basis set of shell 2 is cc-pVDZ, and the basis sets of shell 1 are cc-pVDZ, cc-pVTZ and aug-cc-pVDZ. All calculations result in a dipole moment of 2.17 D, which is 0.02–0.03 D higher than that of the STO-3G in shell 2 calculations. We further see that changing the basis

Table 4 Dipole moment for the target region (central NH$_3$ molecule) computed for a cluster containing 143 molecules, using different basis sets for shell 1 and 2

Basis (shell 1)	Basis (shell 2)	Dipole moment [D]
STO-3G	STO-3G	2.14
cc-pVDZ	STO-3G	2.15
cc-pVTZ	STO-3G	2.15
aug-cc-pVDZ	STO-3G	2.14
aug-cc-pVTZ	STO-3G	2.14
cc-pVDZ	cc-pVDZ	2.17
cc-pVTZ	cc-pVDZ	2.17
aug-cc-pVDZ	cc-pVDZ	2.17
cc-pVTZ	cc-pVTZ	2.17
aug-cc-pVDZ	aug-cc-pVDZ	2.16

The basis sets used for the target region and shell 3+ are aug-cc-pVTZ and STO-3G, respectively

set in shell 2 to cc-pVTZ and aug-cc-pVDZ, the computed dipole moment stays at 2.16–2.17 D. Considering the mean absolute error in Hartree–Fock dipole moments for molecules is found to be 0.16 D [56], these variations are negligible. Hence, it can be concluded that the the basis sets used in shell 1 and 2 has a negligible effect on the dipole moment of the target region. This should be seen in context with the reasonably large basis set (aug-cc-pVTZ) used for the target region. The large basis set of the target region ensures that we do not rely on a large basis set in shell 1 to improve the description of the target region.

4.2.2 Effect of basis set on CC2-in-HF vertical excitation energies

In this section we explore how changing the basis set of shell 1 and 2 affects CC2-in-HF excitation energies, as well as the effect of increasing the active virtual space to also include shell 2. In contrast to the Hartree–Fock dipole moment which only relies on the electronic density in the target region, the excitation energies further requires an active virtual space which extends beyond the target region. Hence, basis set effects is expected to be important here.

Results for how the excitation energies are affected by varying the basis set of shell 1 and 2 is presented in Table 5. The excitation energies are computed for the cluster containing 143 molecules, with aug-cc-pVTZ being used for the target region (central NH$_3$ molecule) and STO-3G being used for shell 3+ (see Sect. 3.2). The occupied active region is set to the target region, while the virtual active region is set to either the target region + shell 1 or the target region + shell 1–2 (see Sect. 3.4).

We first consider the results for which STO-3G is used for shell 2. We see that calculations using target + shell 1 and target + shell 1-2 as active virtual region yields identical results with respect to varying the basis set of shell 1. Increasing the basis set of shell 1 from STO-3G to cc-pVDZ reduces the excitation energy by 0.20 eV. Increasing the basis set of shell 1 from cc-pVDZ to cc-pVTZ, however, does not change the excitation energies. Increasing the basis set of shell 1 to aug-cc-pVDZ and

Table 5 CC2 $S_0 \rightarrow S_1$ excitation energies (eV) showing the effect of varying the basis set of shell 1 and 2, using either the target region + shell 1 or the target region + shell 1–2 as the virtual active region

Basis (shell 1)	Basis (shell 2)	Virtual active region	
		Target + Shell 1	Target + Shell 1–2
STO-3G	STO-3G	9.26	9.26
DZ	STO-3G	9.06	9.06
TZ	STO-3G	9.06	9.06
aDZ	STO-3G	9.03	9.03
aTZ	STO-3G	9.03	9.03
DZ	DZ	9.07	9.06
TZ	DZ	9.07	9.05
aDZ	DZ	9.05	9.04
TZ	TZ	9.07	9.05
aDZ	aDZ	9.05	9.03

All calculations are performed for the cluster containing 143 molecules, with the target region set as the occupied active region and aug-cc-pVTZ and STO-3G being used for the target region and shell 3+, respectively

aug-cc-pVTZ yields an excitation energy 0.03 eV lower than when using cc-pVDZ to cc-pVTZ in shell 1. We therefore see that the basis set of shell 1 one must be of sufficient size, but that increasing the basis set of shell 1 beyond cc-pVDZ gives only modest changes in the excitation energies.

We next consider the results which go beyond STO-3G in shell 2. As seen from Table 5 the excitation energies are increased by between 0.00 and 0.02 eV relative to the results where STO-3G is used in shell 2. This is the case both when the active virtual region is target + shell 1 as well as when the active virtual region is target + shell 1–2. From this we see two main points; (1) the basis set quality in shell 1 is of greater importance than the quality of the basis set in shell 2, and (2) increasing the virtual region beyond shell 1 is of little importance even when using reasonably large (aug-cc-pVDZ) basis sets in shell 2. It therefore appears that the smaller virtual active region (target and shell 1) is sufficient to obtain converged excitation energies with respect to the virtual space. Note that since only the occupied space for the target region is included, no occupied relaxation effects are taken into account.

5 Conclusion

In this paper we use local occupied and virtual orbital spaces for cluster models of a NH_3 crystal to show the convergence characteristics of the Hartree–Fock energy and electronic density in a small target region (single NH_3 molecule). The size of the cluster models ranges from 13 to 953 NH_3 molecules. The calculations illustrate that although the energy of a target region will not converge with cluster size, the energy contribution which only depends on the electronic density of the target region will. Based on this it can be concluded that the electron density of the target region

converges and as a consequence local size-intensive properties may be computed. The convergence of the target electronic density with respect to cluster size yields the possibility to evaluate how the density (and hence properties) is affected by basis set choices in shells around the target region. The properties used for these numerical illustrations are the Hartree–Fock electric dipole moment of the target region, which only relies on the electronic density matrix and local CC2-in-HF vertical excitation energies, which also relies on the virtual space.

Since the electronic density converges with cluster size, so do the target region Hartree–Fock dipole moments. Converged values are obtained using approximately three shells around the central NH_3 molecule. We further show that the effect of quality of the basis set used in the shells outside the target region is negligible for the dipole moment calculations. Using a minimal basis seems to be sufficient to capture the long range effects of the shells on the electronic density of the target region. The lowest singlet CC2-in-HF vertical excitation energies are also seen to converge with cluster size and basis set, despite the fact that the ground state Hartree–Fock energy does not converge with cluster size. Excitation energies using occupied and virtual spaces spanning the target region and the target region + shell 1, respectively, show convergence with cluster size with only small variations beyond three shells. Increasing the virtual space beyond shell 1 is seen to effect the excitation energies in the order of 0.00–0.02 eV. Unlike for the dipole moment, the excitation energies requires that the basis set of shell 1 is of sufficient size, but the quality of the basis set for shells beyond has little effect. For the vertical excitation energies presented, it is important to note that the occupied space only comprise of the occupied space of the target region (the central NH_3 molecule). Including a larger occupied space would result in relaxation effects which would lead to lower excitation energies. However, the intention of this study is not to obtain quantitative accuracy in the lowest local excitation of the NH_3 crystal, but rather to illustrate the cluster and basis set dependencies of the excitation energies.

The paper thus demonstrates fundamental aspects relating to the convergence of electronic density of a target region, and hence local size-intensive properties, with respect to cluster size. It is therefore not necessary to require an infinite system and converged energy to compute size-intensive properties for a target region of a molecular crystal using the electronic density. We further see that although the cluster needs to be of a given size to obtain a converged electronic density in the target region, a minimal basis description of the outer shells are sufficient to capture the correct interaction with the target region. The concepts illustrated in this paper are attainable using any fragmentation or orbital space partitioned based approach, as long as it contain the effective interaction between the target region and the rest of the cluster.

Supplementary information Geometries of the clusters for presented results are available at https://dataverse.no/dataverse/ntnu. with DOI https://doi.org/10.18710/UOTXTK.

References

1. W. Kohn, Density functional and density matrix method scaling linearly with the number of atoms. Phys. Rev. Lett. **76**, 3168–3171 (1996). https://doi.org/10.1103/PhysRevLett.76.3168
2. W. Yang, Direct calculation of electron density in density-functional theory. Phys. Rev. Lett. **66**, 1438–1441 (1991). https://doi.org/10.1103/PhysRevLett.66.1438
3. E. Prodan, W. Kohn, Nearsightedness of electronic matter. Proc. Natl. Acad. Sci. **102**, 11635–11638 (2005). https://doi.org/10.1073/pnas.0505436102
4. I. Zhang, J. Jiang, B. Gao, X. Xu, Y. Luo, RRS-PBC: a molecular approach for periodic systems. Sci. China Chem. **57**, 1–6 (2014). https://doi.org/10.1007/s11426-014-5183-y
5. C. Huang, Embedded cluster density approximation for exchange-correlation energy: a natural extension of the local density approximation. J. Chem. Theory Comput. **14**, 6211–6225 (2018). https://doi.org/10.1021/acs.jctc.8b00471
6. M. Marsman, A. Grüneis, J. Paier, G. Kresse, Second-order Møller-Plesset perturbation theory applied to extended systems. I. Within the projector-augmented-wave formalism using a plane wave basis set. J. Chem. Phys. **130**, 184103 (2009). https://doi.org/10.1063/1.3126249
7. E. Rebolini, G. Baardsen, A.S. Hansen, K.R. Leikanger, T.B. Pedersen, Divide-expand-consolidate second-order Møller-Plesset theory with periodic boundary conditions. J. Chem. Theory Comput. **14**, 2427–2438 (2018). https://doi.org/10.1021/acs.jctc.8b00021
8. J. McClain, Q. Sun, G.K.L. Chan, T.C. Berkelbach, Gaussian-based coupled-cluster theory for the ground-state and band structure of solids. J. Chem. Theory Comput. **13**, 1209–1218 (2017). https://doi.org/10.1021/acs.jctc.7b00049
9. C. Pisani, M. Busso, G. Capecchi, S. Casassa, R. Dovesi, L. Maschio, C. Zicovich-Wilson, M. Schütz, Local-MP2 electron correlation method for nonconducting crystals. J. Chem. Phys. **122**, 094113 (2005). https://doi.org/10.1063/1.1857479
10. C. Edmiston, K. Ruedenberg, Localized atomic and molecular orbitals. Rev. Mod. Phys. **35**, 457–464 (1963). https://doi.org/10.1103/RevModPhys.35.457
11. S.F. Boys, Construction of some molecular orbitals to be approximately invariant for changes from one molecule to another. Rev. Mod. Phys. **32**, 296–299 (1960). https://doi.org/10.1103/RevModPhys.32.296
12. J. Pipek, P.G. Mezey, A fast intrinsic localization procedure applicable for ab initio and semiempirical linear combination of atomic orbital wave functions. J. Chem. Phys. **90**, 4916–4926 (1989). https://doi.org/10.1063/1.456588
13. P. Pulay, Localizability of dynamic electron correlation. Chem. Phys. Lett. **100**, 151–154 (1983). https://doi.org/10.1016/0009-2614(83)80703-9
14. C. Edmiston, M. Krauss, Pseudonatural orbitals as a basis for the superposition of configurations. I. He2+. J. Chem. Phys. **45**, 1833–1839 (1966). https://doi.org/10.1063/1.1727841
15. W. Meyer, Ionization energies of water from PNO-CI calculations. Int. J. Quantum Chem. **5**, 341–348 (1971). https://doi.org/10.1002/qua.560050839
16. W. Meyer, PNO-CI studies of electron correlation effects. I. Configuration expansion by means of nonorthogonal orbitals, and application to the ground state and ionized states of methane. J. Chem. Phys. **58**, 1017–1035 (1973). https://doi.org/10.1063/1.1679283
17. I.M. Høyvik, R.H. Myhre, H. Koch, Correlated natural transition orbitals for core excitation energies in multilevel coupled cluster models. J. Chem. Phys. **146**, 144109 (2017). https://doi.org/10.1063/1.4979908
18. C. Krause, H.J. Werner, Comparison of explicitly correlated local coupled-cluster methods with various choices of virtual orbitals. Phys. Chem. Chem. Phys. **14**, 7591–7604 (2012). https://doi.org/10.1039/C2CP40231A
19. A.S. Hansen, G. Baardsen, E. Rebolini, L. Maschio, T.B. Pedersen, Representation of the virtual space in extended systems—a correlation energy convergence study. Mol. Phys. **118**, e1733118 (2020). https://doi.org/10.1080/00268976.2020.1733118

20. I.M. Høyvik, The spectrum of the atomic orbital overlap matrix and the locality of the virtual electronic density matrix. Mol. Phys. **118**, e1765034 (2020). https://doi.org/10.1080/00268976.2020.1765034

21. H. Stoll, Correlation energy of diamond. Phys. Rev. B **46**, 6700–6704 (1992). https://doi.org/10.1103/PhysRevB.46.6700

22. S. Saebo, P. Pulay, Local treatment of electron correlation. Annu. Rev. Phys. Chem. **44**, 213–236 (1993). https://doi.org/10.1146/annurev.pc.44.100193.001241

23. S.R. Gadre, R.N. Shirsat, A.C. Limaye, Molecular tailoring approach for simulation of electrostatic properties. J. Phys. Chem. **98**, 9165–9169 (1994). https://doi.org/10.1021/j100088a013

24. C. Hampel, H. Werner, Local treatment of electron correlation in coupled cluster theory. J. Chem. Phys. **104**, 6286–6297 (1996). https://doi.org/10.1063/1.471289

25. P. Maslen, M. Head-Gordon, Non-iterative local second order Møller-Plesset theory. Chem. Phys. Lett. **283**, 102–108 (1998). https://doi.org/10.1016/S0009-2614(97)01333-X

26. M. Schütz, G. Hetzer, H.J. Werner, Low-order scaling local electron correlation methods. I. Linear scaling local MP2. J. Chem. Phys. **111**, 5691–5705 (1999). https://doi.org/10.1063/1.479957

27. K. Kitaura, E. Ikeo, T. Asada, T. Nakano, M. Uebayasi, Fragment molecular orbital method: an approximate computational method for large molecules. Chem. Phys. Lett. **313**, 701–706 (1999). https://doi.org/10.1016/S0009-2614(99)00874-X

28. G.E. Scuseria, P.Y. Ayala, Linear scaling coupled cluster and perturbation theories in the atomic orbital basis. J. Chem. Phys. **111**, 8330–8343 (1999). https://doi.org/10.1063/1.480174

29. S. Li, J. Ma, Y. Jiang, Linear scaling local correlation approach for solving the coupled cluster equations of large systems. J. Comput. Chem. **23**, 237–244 (2002). https://doi.org/10.1002/jcc.10003

30. M. Schütz, A new, fast, semi-direct implementation of linear scaling local coupled cluster theory. Phys. Chem. Chem. Phys. **4**, 3941–3947 (2002). https://doi.org/10.1039/B203994J

31. T. Crawford, R.A. King, Locally correlated equation-of-motion coupled cluster theory for the excited states of large molecules. Chem. Phys. Lett. **366**, 611–622 (2002). https://doi.org/10.1016/S0009-2614(02)01639-1

32. N. Flocke, R.J. Bartlett, A natural linear scaling coupled-cluster method. J. Chem. Phys. **121**, 10935–10944 (2004). https://doi.org/10.1063/1.1811606

33. S. Hirata, M. Valiev, M. Dupuis, S.S. Xantheas, S. Sugiki, H. Sekino, Fast electron correlation methods for molecular clusters in the ground and excited states. Mol. Phys. **103**, 2255–2265 (2005). https://doi.org/10.1080/00268970500083788

34. D. Kats, T. Korona, M. Schütz, Local CC2 electronic excitation energies for large molecules with density fitting. J. Chem. Phys. **125**, 104106 (2006). https://doi.org/10.1063/1.2339021

35. O. Christiansen, P. Manninen, P. Jørgensen, J. Olsen, Coupled-cluster theory in a projected atomic orbital basis. J. Chem. Phys. **124**, 084103 (2006). https://doi.org/10.1063/1.2173249

36. J.E. Subotnik, A. Sodt, M. Head-Gordon, A near linear-scaling smooth local coupled cluster algorithm for electronic structure. J. Chem. Phys. **125**, 074116 (2006). https://doi.org/10.1063/1.2336426

37. J. Friedrich, M. Hanrath, M. Dolg, Fully automated implementation of the incremental scheme: application to CCSD energies for hydrocarbons and transition metal compounds. J. Chem. Phys. **126**, 154110 (2007). https://doi.org/10.1063/1.2721538

38. M. Kobayashi, H. Nakai, Extension of linear-scaling divide-and-conquer-based correlation method to coupled cluster theory with singles and doubles excitations. J. Chem. Phys. **129**, 044103 (2008). https://doi.org/10.1063/1.2956490

39. F. Neese, F. Wennmohs, A. Hansen, Efficient and accurate local approximations to coupled-electron pair approaches: an attempt to revive the pair natural orbital method. J. Chem. Phys. **130**, 114108 (2009). https://doi.org/10.1063/1.3086717

40. M. Ziółkowski, B. Jansík, T. Kjærgaard, P. Jørgensen, Linear scaling coupled cluster method with correlation energy based error control. J. Chem. Phys. **133**, 014107 (2010). https://doi.org/10.1063/1.3456535

41. Z. Rolik, M. Kállay, A general-order local coupled-cluster method based on the cluster-in-molecule approach. J. Chem. Phys. **135**, 104111 (2011). https://doi.org/10.1063/1.3632085

42. J. Yang, G.K.L. Chan, F.R. Manby, M. Schütz, H.J. Werner, The orbital-specific-virtual local coupled cluster singles and doubles method. J. Chem. Phys. **136**, 144105 (2012). https://doi.org/10.1063/1.3696963

43. S. Sæther, T. Kjærgaard, H. Koch, I.M. Høyvik, Density-based multilevel Hartree-Fock model. J. Chem. Theory Comput. **13**, 5282–5290 (2017). https://doi.org/10.1021/acs.jctc.7b00689

44. S. Høst, J. Olsen, B. Jansík, L. Thøgersen, P. Jørgensen, T. Helgaker, The augmented Roothaan-Hall method for optimizing Hartree-Fock and Kohn-Sham density matrices. J. Chem. Phys. **129**, 124106 (2008). https://doi.org/10.1063/1.2974099

45. I.M. Høyvik, Convergence acceleration for the multilevel Hartree-Fock model. Mol. Phys. **118**, 1626929 (2020). https://doi.org/10.1080/00268976.2019.1626929

46. T. Helgaker, P. Jørgensen, J. Olsen, *Molecular Electronic Structure Theory*, 1st edn. (Wiley, New York, 2000)

47. I.M. Høyvik, K. Kristensen, T. Kjaergaard, P. Jørgensen, A perspective on the localizability of Hartree-Fock orbitals. Theoret. Chem. Acc. (2014). https://doi.org/10.1007/s00214-013-1417-x

48. K. Aidas, C. Angeli, K.L. Bak, V. Bakken, R. Bast, L. Boman, O. Christiansen, R. Cimiraglia, S. Coriani, P. Dahle, E.K. Dalskov, U. Ekström, T. Enevoldsen, J.J. Eriksen, P. Ettenhuber, B. Fernández, L. Ferrighi, H. Fliegl, L. Frediani, K. Hald, A. Halkier, C. Hättig, H. Heiberg, T. Helgaker, A.C. Hennum, H. Hettema, E. Hjertenæs, S. Høst, I.M. Høyvik, M.F. Iozzi, B. Jansík, H.J.A. Jensen, D. Jonsson, P. Jørgensen, J. Kauczor, S. Kirpekar, T. Kjærgaard, W. Klopper, S. Knecht, R. Kobayashi, H. Koch, J. Kongsted, A. Krapp, K. Kristensen, A. Ligabue, O.B. Lutnæs, J.I. Melo, K.V. Mikkelsen, R.H. Myhre, C. Neiss, C.B. Nielsen, P. Norman, J. Olsen, J.M.H. Olsen, A. Osted, M.J. Packer, F. Pawlowski, T.B. Pedersen, P.F. Provasi, S. Reine, Z. Rinkevicius, T.A. Ruden, K. Ruud, V.V. Rybkin, P. Sałek, C.C.M. Samson, A.S. de Merás, T. Saue, S.P.A. Sauer, B. Schimmelpfennig, K. Sneskov, A.H. Steindal, K.O. Sylvester-Hvid, P.R. Taylor, A.M. Teale, E.I. Tellgren, D.P. Tew, A.J. Thorvaldsen, L. Thøgersen, O. Vahtras, M.A. Watson, D.J.D. Wilson, M. Ziolkowski, H. Ågren, The Dalton quantum chemistry program system. WIREs Comput. Mol. Sci. **4**, 269–284 (2014). https://doi.org/10.1002/wcms.1172

49. B. Jansík, S. Høst, K. Kristensen, P. Jørgensen, Local orbitals by minimizing powers of the orbital variance. J. Chem. Phys. **134**, 194104 (2011). https://doi.org/10.1063/1.3590361

50. S.D. Folkestad, E.F. Kjønstad, R.H. Myhre, J.H. Andersen, A. Balbi, S. Coriani, T. Giovannini, L. Goletto, T.S. Haugland, A. Hutcheson, I.M. Høyvik, T. Moitra, A.C. Paul, M. Scavino, A.S. Skeidsvoll, Å.H. Tveten, H. Koch, eT 1.0: an open source electronic structure program with emphasis on coupled cluster and multilevel methods. J. Chem. Phys. **152**, 184103 (2020). https://doi.org/10.1063/5.0004713

51. S.D. Folkestad, E.F. Kjønstad, H. Koch, An efficient algorithm for Cholesky decomposition of electron repulsion integrals. J. Chem. Phys. **150**, 194112 (2019). https://doi.org/10.1063/1.5083802

52. A.W. Hewat, C. Riekel, The crystal structure of deuteroammonia between 2 and 180 K by neutron powder profile refinement. Acta Crystallogr. A **35**, 569–571 (1979). https://doi.org/10.1107/S0567739479001340

53. T.H. Dunning, Gaussian basis sets for use in correlated molecular calculations. I. The atoms boron through neon and hydrogen. J. Chem. Phys. **90**, 1007–1023 (1989). https://doi.org/10.1063/1.456153

54. R. Ditchfield, W.J. Hehre, J.A. Pople, Self-consistent molecular-orbital methods. IX. An extended gaussian-type basis for molecular-orbital studies of organic molecules. J. Chem. Phys. **54**, 724–728 (1971). https://doi.org/10.1063/1.1674902

55. I.M. Høyvik, B. Jansik, P. Jørgensen, Trust region minimization of orbital localization functions. J. Chem. Theory Comput. **8**, 3137–3146 (2012). https://doi.org/10.1021/ct300473g

56. K.L. Bak, J. Gauss, T. Helgaker, P. Jørgensen, J. Olsen, The accuracy of molecular dipole moments in standard electronic structure calculations. Chem. Phys. Lett. **319**, 563–568 (2000). https://doi.org/10.1016/S0009-2614(00)00198-6

57. M. Själander, M. Jahre, G. Tufte, N. Reissmann. EPIC: an energy-efficient, high-performance GPGPU computing research infrastructure (2019)